

Journal Pre-proofs

A Deep Convolutional Neural Network based Computer Aided Diagnosis System for the Prediction of Alzheimer's Disease in MRI Images

V. Sathiyamoorthi, A.K. Ilavarasi, K. Murugeswari, Syed Thouheed Ahmed, B. Aruna Devi, Murali Kalipindi

PII: S0263-2241(20)31331-2
DOI: <https://doi.org/10.1016/j.measurement.2020.108838>
Reference: MEASUR 108838

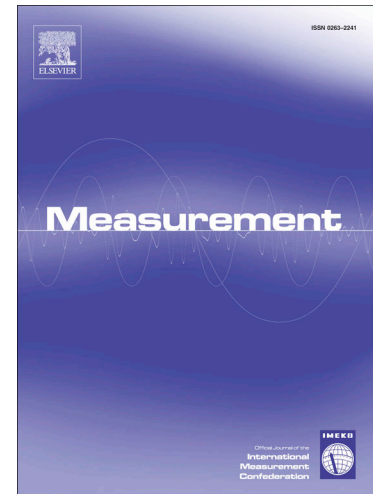
To appear in: *Measurement*

Received Date: 4 June 2020
Revised Date: 25 November 2020
Accepted Date: 6 December 2020

Please cite this article as: V. Sathiyamoorthi, A.K. Ilavarasi, K. Murugeswari, S. Thouheed Ahmed, B. Aruna Devi, M. Kalipindi, A Deep Convolutional Neural Network based Computer Aided Diagnosis System for the Prediction of Alzheimer's Disease in MRI Images, *Measurement* (2020), doi: <https://doi.org/10.1016/j.measurement.2020.108838>

This is a PDF file of an article that has undergone enhancements after acceptance, such as the addition of a cover page and metadata, and formatting for readability, but it is not yet the definitive version of record. This version will undergo additional copyediting, typesetting and review before it is published in its final form, but we are providing this version to give early visibility of the article. Please note that, during the production process, errors may be discovered which could affect the content, and all legal disclaimers that apply to the journal pertain.

© 2020 Published by Elsevier Ltd.



1 **A Deep Convolutional Neural Network based Computer Aided Diagnosis System for the**
2 **Prediction of Alzheimer's Disease in MRI Images**

3 Sathiyamoorthi V^{1*}, Ilavarasi A K², Murugeswari K³, Syed Thouheed Ahmed⁴, Aruna Devi B⁵, Murali
4 Kalipindi⁶

5 *¹Department of CSE, Sona College of Technology, Salem-5, TN, India.*

6 *²Division of Healthcare Advancement, Innovation and Research, Vellore Institute of Technology,*
7 *Chennai, TN, India.*

8 *³Department of CSE, Kalasalingam Academy of Research and Education, Krishnankovil, TN, India.*

9 *⁴Department of CSE, Dr T Thimmaiah Institute of Technology, Oorgaum, Kolar Gold Field, KA, India.*

10 *⁵ Department of ECE, Dr.N.G.P. Institute of Technology, Coimbatore, TN, India.*

11 *⁶Department of ECE, Vijaya Institute of Technology for Women, Enikepadu, Vijayawada, AP, India.*

12
13 **Corresponding Author: Sathiyamoorthi V, sathyait2003@gmail.com*
14

- 15 • A CAD system is proposed to detect and classify Alzheimer Disease on MRI real image
- 16 • Uses MRI differentiation method to differentiate the tumor from the non-tumor cells
- 17 • Image preprocessing is performed using 2D-ABF and AHA algorithms
- 18 • Image segmentation is done to retrieve ROI using MEM algorithm
- 19 • Features are retrieved using GLCM and DCNN is to classify normal and abnormal image

20

Journal Pre-proofs

21

22 **ABSTRACT**

23 In the recent past, biomedical domain has become popular due to digital image processing of
24 accurate and efficient diagnosis of clinical patients using Computer-Aided Diagnosis (CAD). Appropriate
25 and punctual disease identification and treatment arrangement directs to enhance superiority of life and
26 improved life hope in Alzheimer Disease (AD) patients. The cutting-edge approaches that believe
27 multimodal analysis have been shown to be efficient and accurate are improved compared with manual
28 analysis. Many tools have been introduced for detection of Alzheimer but still it is a financially high costly
29 diagnosis system gives detection of disease with low accuracy and efficient due to performance of Magnetic
30 Resonance Imaging (MRI) scanning devices. A novel methodology is proposed in this research as CAD
31 process using various algorithms for predicting AD. The MRI images from scanning device are a highly
32 noisy image due to thermal activities of hardware involved in scanning device. The image restoration
33 technique is applied using 2D Adaptive Bilateral Filter (2D-ABF) algorithm. The quality of image in terms
34 of brightness and contrast are improved using image enhancement techniques based on Adaptive Histogram
35 Adjustment (AHA) algorithm. The Region of Interest of Alzheimer disease is segmented using Adaptive
36 Mean Shift Modified Expectation Maximization (AMS-MEM) algorithm. The various features are
37 calculated using second order 2-Dimensional Gray Level Co-Occurrence Matrix (2D-GLCM). Based on
38 selection of features, the Deep Learning (DL) approach is used to classify the disease images and its stages.
39 The Deep Convolutional Neural Network (DCNN) is the classification technique implemented to classify
40 disease for proper diagnostic decision making. The experimental results prove that the proposed
41 methodology provides better accuracy and efficiency than existing system.

42 **Keywords:** CAD, MRI, 2D-ABF, AHA, GLCM, ML, DL

43

44 **1. INTRODUCTION**

45 Computer Aided Diagnosis (CAD) is an attractive subject of studies into Alzheimer's disease (AD).
46 A fairly broad training database is used to base several implementations. Limited hospitals, however, are
47 typically unable to obtain enough materials for rigorous identification training. Although the exchange of
48 information in scientific research is growing, it is unclear if a system based on one database is very well
49 adapted for other resources. Compared to a system based on the initial limited dataset, the accuracy
50 improved by around 20 per cent. The results showed that the proposed solution is an innovative and efficient
51 method of CAD in clinics only with limited data set for learning. Continuous work is under way to
52 accurately diagnose AD focused on conventional deep learning methods, and its related strategies have
53 become a common alternative for AD diagnostics [1]. However, it is time-consuming and difficult to gather
54 evidence from various modalities, and certain modalities may have side effects on radioactivity. The object
55 of our research is systemic Magnetic Resonance Imaging (sMRI). Their aims are as follows: 1) to improve
56 the degree of precision equivalent to the cutting-edge approaches; 2) to address the question of overcoming
57 and; 3) to examine established brain indications that have perceptible AD diagnostic functionality. The
58 specificity of an AD assessment relies largely upon the disease biological markers.

59 During the early stages of AD, hippo-campal shrinkage is specified which has an established
60 association with memory loss [2]. A very common and successful method for diagnosing AD is systemic
61 MRI analysis. The effectiveness of software-aided models of diagnostic using brain MRI image largely
62 depends on factors such as steps: 1) nonlinear identification through content of image, 2) clustering of
63 tissues in brain. For addressing constraint a method is proposed for removal of landmark dependent features
64 that does not involve nonlinear identification and clustering of tissues. An innovative neighborhood filter
65 that retains edge is suggested for image filtering. The filter's key objective is a hybrid de-noising feature in
66 order to compensate quality of image although attempting to retain edge of the image [3].

67 The proposed method uses image boundaries to filter the region in an edge-conserving way.
68 Response of a variable, in a pixel region, in filtering, relies on the region between the object and the sensor.
69 In addition, the measurement edge between it and the pixel does not lead to the calculation of the gray point
70 image average decreases vibration which has other damaging consequences content blurring. During noise
71 level low, the impact of content in image loss may be higher than the impact of noise cancellation and
72 grouping of the initial image yields better results than grouping the normal image [4]. Computer
73 representations findings demonstrate that the approach overcomes the drawbacks of modern approaches
74 based on calculations of the vector image efficiency. It is also narrative basic and fast to deploy [5].

75 The paradigm of MRI is an effective approach for brain analysis. While collection, MRI brain
76 images could be integrated through interference that decreases image quality with limits the diagnostic
77 efficiency and accuracy. Eliminating noise of clinical images is an essential activity in per-processing and
78 various approaches occur to remove noise in clinical images. Various de-noising methods such as non-local
79 measures, important element investigation, bilateral and temporally high adaptive non-local means
80 (TANLM) filter is analyzed in this work to remove noise in MR. A structural association histogram is a
81 grayscale-based study of the pixel brightness distribution degree by creating histogram correlation which
82 could be increased effective contrast improvement in different artifacts. Approach achieves important
83 effects during pre-processing of contrast improvement and encourages corresponding CAD procedures,
84 thus reducing the time for detection and increasing accuracy. Popular approaches for improving contrast
85 images include histogram equalization (HE) and selective eclipse of the adaptive histogram (CLAHE). HE
86 builds up the image pixel elements values histogram in image depends to the initial exported MRI brain
87 image shows every pixel element functions in the image. It also adjusts the initial pixel quantities to increase
88 the contrast between the images [6].

89 The dynamic model focuses on individual artifacts to reflect the pixel similarity functions for
90 optimization and governs the intensity of each single entity in an evolutionary way [7]. Thus, implementing
91 the segmentation of medical data remains a constant difficult task that has attracted a few researchers'
92 attention in the last year. MRI differentiation is implemented to region of interest. The concept is to treat
93 this issue as a classification task in which the goal is to differentiate among normal and abnormal elements
94 on MRI image based on several characteristics, including levels of intensity and shape. More specifically,
95 suggest using Support Vector Machine (SVM) and are within common and well-motivated classification
96 techniques [8]. The deep neural network is an evolving method of deep learning, which has verified its
97 suitability for different image classification. Particularly, the CNN controls different picture recognition
98 tasks for better performances. Clinical image databases, though, are challenging to obtain as they need a
99 great deal of technical experience to mark. The research explores how the CNN related algorithm can be
100 extended to a chest X-ray dataset to identify pneumonia.

101 These are kernel support vector machine classification with local free spinning and direction
102 characteristics, transferring learning from ground up on two CNN models: probabilistic neural Group i.e.,
103 VGG16 and Inception V3, and module network training. Information raise is a form of pre-processing data
104 and is applicable to all three processes. Results from the experiments indicate that information increase is
105 usually an efficient way to boost efficiency for all three algorithms. Transfer learning is also a more efficient
106 form of identification on a restricted database when opposed to a help support vector with stable, isolated
107 basic characteristics and capsule network based fast and Rotating Binary (RB). Retraining of particular
108 applications on a current goal set of data is vital for achieving efficiency in transfer learning. And, the
109 second important factor is an appropriate difficulty of the system which fits the set of data measure
110 [9]. Statistical method of several neurological diseases varies depending on the computerized and precise
111 differentiation and structural categorization. Because of their self-learning functionality over vast quantities
112 of set of data, the DL based recognition and segmentation system have obtained research interest nowadays.
113 Convolutional neural network (CNN) needs to take preprocessed feature maps in the Curvelet framework
114 to categorize the set of data for the MRI brain image. Curvelets have improved feature vector and due to its
115 multi-directional functionality, the extracted features are much more accurate than conventional wavelet
116 transformation. Next, the methods of differentiation to research anatomical structures and location of brain
117 tumors are dealt with and finally the CNN quality is mentioned. The function extraction in the Curvelet
118 domain and CNN offer an improvement in precision compared with the wavelet transformation and
119 identification utilizing conventional classification techniques such as SVM and Probabilistic Neural
120 Network (PNN) [10]. In this research paper, section 2 consists of related works of various researchers and
121 motivation behind this work is given. The proposed system is elaborated in section 3 and then experimental
122 results are shown in section 4. Finally, section 5 concludes the entire research with future work.

123 2. RELATED WORKS

124 Krystyna Malik, et. al [11] has proposed the filter design was a refinement of bilateral de-noising
125 methodology that obtains relation resemblance color pixels elements and temporal range of pixel elements.
126 Rather than direct measurement of the dissimilarity factor, therefore, the cost of a link is measured across
127 a digital route that connects the fundamental pixel of the processing window and its surroundings. As in the
128 traditional bilateral filter, the filter performance was measured like weighted standard of the pixels that
129 have local relationship through de-noising window and weights vectors are components of the marginal
130 contact element. The most commonly used filtering models are focused on the Vector Median Filter (VMF)
131 method, whose performance is determined using the vector organizing principle for a collection of pixels
132 from the processing window. Sorting the accumulated ranges from a specified pixel to all other pixels
133 through the filtering window determines the sorting of the vectors.

134 Jun Wang, et. al [12] has discussed various component-based transforms for momentum and
135 magnetic data sets that can be used to illustrate related functionality. Nearly all of them, though, face the
136 uncertainty issue in differential estimation. Hence, noise removal is sometimes implemented before
137 implementing component-based transforms to increase the accuracy of the results. V. Anoop1, et. al [13]
138 has proposed the impulse noise and Rician noise using Bilateral Filter (BF) the clinical MR images are
139 eliminated. Improved grasshopper simulation methodology (EGOA) is used to refine the BF variables. The
140 occurred impulse and Rician noises are used to mimic the clinical MR images (with varying differences).
141 In checking regions of window height, space and strength scope, the EGOA is added to the noisy image in
142 order to get the filter specifications efficiently. For optimization, the PSNR is used as the health benefit.

143 After maximum certainty of variables, it is analyzed the proposed effects of the methodology with other
144 MR images. The findings of the suggested de-noising approach are compared with other previously used
145 BFs, genetic algorithm (GA), generalized search algorithm (GSA) utilizing consistency parameters such as
146 Signal-to-Noise Ratio (SNR), the image quality measuring metric is structural similarity index metric
147 (SSIM), error parameter is mean squared error (MSE) and Peak Signal to Noise Ratio (PSNR) to explain
148 choice value of image quality measuring parameters.

149 The surroundings weighted average of the pixel is used to remove the pixel. For this equation, the
150 weights can be obtained by the physical and magnitude range of a pixel from its region. In a pixel
151 neighborhood the spectral range is defined with the parameters of the field (spatial) filter while the weights
152 of the filter set (intensity) are proportional to the isotopic range of the pixel. Rinkal Patel et. al [14] has
153 designed the AD neuro-imaging research was the most popular technique, where different brain
154 regions/voxels are studied independently. Such methods are successful in other situations. However, they
155 did not shed light on the interaction of the inner brain region correlated with brain activity or fascinating
156 illness. Human brain is, in essence, anatomically a rather complicated organ and the functional connections
157 among its regions are much more so. Consequently, comprehension of this interdependence or connectivity
158 between brain regions is required. The deep learning methodology named "Sparse Inverse Covariance
159 Analysis" for learning functionality in the brain field, with limited computing expense and densely the
160 correct degree. Within Gaussian hypothesis, any dimension of the vector of reverse covariance expresses
161 conditional dependency between the pair of variables in the constituent, provided all parameters. Through
162 implementing sparsely restriction, excessive/noisy structural constraints are abolished through placing the
163 component factor at zero, participating in the factor pairs becoming conditionally autonomous [22], [23].

164 All radioactive MRI and FDG-PET may be used to support doctors in the diagnostic process, i.e.
165 assessing the brain regions and classifying the disease as Normal Controls (NC's), MCI (Mild Cognitive
166 Impairment), AD or any other Alzheimer struggling. Diagram representation of image data is a moment
167 operation and often vulnerable to mistake. The visual assessment has been suggested with mathematical
168 methods in location (or in comparison to).Mostafa Amin-Naji, et. al [15] has proposed the Deep learning
169 (DL) approaches currently have been used in the detection and diagnosis of radiography and have greatly
170 enhanced method efficiency. Since Alzheimer's disease (AD) is among the most financially costly
171 disorders, several scholars have focused on developing a high precision software system for the diagnosis
172 of AD and Normal Control (NC) instances. A modern computational approach focused on deep learning is
173 used for diagnosing Alzheimer's disease. Here between DL networks, the Siamese Convolution Neural
174 Network (SCNN) is introduced with triple ResNet-34 divisions to differentiate through the Structural MRI
175 among the AD and the NC. A SCNN comprises rather than two CNN groups which are mostly similar to
176 each other. The division contains convolution sequence, ReLU, accumulating, and totally linked surfaces.
177 These dual-branches of CNNs are concurrently training on multiple image objects and are generating
178 segments of the same direction function. The similitude of input objects is obtained by measuring the
179 resemblance and range of the variables of the source function.

180 The negative image is likewise the randomly chosen item from the same anchor image mark. It has
181 been common to assess Alzheimer's disease (AD) from moderate cognitive disorder (MCI) and executive
182 norm (CN). Recent neuro-imaging developments in acceptance of machine-learning technologies are
183 particularly useful for pattern analysis in radiography to assist the doctor in early detection of AD. Early
184 pathological brain atrophy and stable brain atrophy are found to be similar. In our endeavor, suggested a

185 model that can more reliably distinguish mild cognitive impairment (MCI) to improve early detection of
186 AD. MRI's are initially split into slides to conduct the clustering of T2 weighted MRI images. Through
187 skull stripped software, the non-brain substances are separated from the frames. Increases in brain shape
188 and appearance are used to distinguish stable and deformed, and improved Independent Component
189 Analysis (ICA) is used to classify brain imaging into WM, GM, and Cerebrospinal Fluid (CSF). Atrophy
190 of the brain tissue is required for the identification of stage AD. AD is a chronic condition, improvements
191 in the brain function perception of GM, structure and thickness of the WM, as well as blood vessel
192 extension. Define the AD in our task, based on GM degeneration. GM includes nerve cell bodies or glial
193 cells, and semi-neuron neurons. GM undergoes production and development during infancy and
194 adolescence; it is used to bring sugar to the brain; perception, voice, and cognitive function improve in this
195 impact. In our research concentrated primarily on the gray matter, in order to identify the AD. It is included
196 CNN as a discriminator from the past few years that is used in various computer perception strategies. The
197 definition of a combination model is implemented in our suggested Hybrid Improved ICA and it is defined
198 in groups which are mutually dependent.

199 Utilizing Markov Random Field (MRF) Cognitive information is applied to Gaussian Mixture
200 Model (GMM) in the updated GMM method and takes into consideration temporal concentration. In
201 Expectation Maximization (EM), Predicted phase is determined using mean log probability and deviation
202 is measured using updated K-mean and endogenous factor is measured using Gibbs volume. The above
203 listed variables are used to conduct clustering of the Brain MRI slides as input variables to HEICA. Shanthi
204 K J., et. al [16] has proposed the quality of brain MRI clustering relies on the precision with which the brain
205 structures are separated from the MR images. While the skull removed image would only have significance
206 in the cerebral regions. Skull grinding may be extended with effectiveness to both convective and axial
207 images. The standard distressed image of the skull has three sections of White Matter (WM), Gray Matter
208 (GM) and Cerebrospinal fluid (CSF) substances. The skull stripped image histogram reveals no clear peaks
209 and troughs referring to certain groups. WM pixels are lighter in T1 weighted images, CSF pixels are
210 darkest, and GM pixels are aligned on a contrast higher side. In the proposed work, weighted vector image
211 data T1 structures are used as the test images. The initial peak is equivalent to white matter, the second
212 peak corresponds to GM and the final peak related to CSF. R. Thillaikkarasi., et. al [17] has investigated brain
213 tumor may be produced by an unpredictable rise in irregular cells in brain tissue and has two forms in
214 cancers: one is harmless and the other is malignant. The benign brain tumor may not influence the adjacent
215 usual and stable tissue however the malignant tumor that influence the adjacent brain tissues, which may
216 contribute to person's death. Early diagnosis of brain tumor could be important to ensure patient life.

217 A deep learning - based algorithm (kernel-based CNN) with M-SVM is introduced for automated
218 and effective segmentation of the tumor. This proposed research involves many measures that include
219 preprocessing, processing of features image identification and brain tumor segmentation. G. K. Reynolds
220 et. al [18] has proposed diffusion MRI (dMRI) modern indications for disease diagnosis not possible using
221 normal anatomical MRI. Here, a novel approach is implemented for designing the signal directly to derive
222 features for classification of Alzheimer's disease (AD) patients against Healthy Control System (HCS).

223 Jun Zhang et. al [19] has proposed structural magnetic resonance imaging (MRI) effective method
224 for Alzheimer's disease (AD) detection. Using these temporal and statistical characteristics, a dynamic
225 support vector machine (SVM) is eventually introduced to separate AD objects or Moderate Cognitive
226 Disability (MCD) samples from Healthy Controls (HCs). Ramy A. Zeineldin et. al [20] has developed

227 DeepSeg, as a structure for modular decoupling. It consists of two main parts linked, centered on a
228 connection of encoding and decoding. The encoder component is a Deep Neural Network (DNN) which is
229 accountable for processing of spatial information. The subsequent semantic graph is placed into the portion
230 of the decoder to get the chart of likelihood of maximum resolution. Various CNN models such as residual
231 neural network (ResNet), deep convolutional network (DenseNet), and NASNet were used based on
232 modified U-Net design. Owing to their malignant existence and accelerated development, Gliomas are the
233 most frequent and violent form of brain tumors. Differentiating cancer cell boundaries from healthy cells
234 continues to be a difficult challenge in medical diagnosis. Fluid-attenuated Inversion Recovery (FLAIR)
235 MRI method could provide tumor diffusion details for the doctor. Runhong Zhang et. al [21] has adopted
236 NGI-ADP surface design for limit equilibrium research, on the basis of which the impacts of soft clay
237 anisotropy on the deformation of the diaphragm wall in approaches to the study is analyzed. It studied
238 quantitatively more than one thousand cases of finite elements, accompanied by substantial numerical
239 simulations.

240 **2.1 Motivation**

241 The AD is a medical illness which produces loss of memory and cognitive impairment by the killing
242 of brain cells. A degenerative form of Alzheimer, the condition begins slightly, and is slowly becoming
243 worse. Brain image processing is a significant field of scientific study, findings for the diagnosis of brain
244 disorders. Small brain function and blood pressure are the primary triggers for Alzheimer's diseases. In
245 specific the procedure of clustering is used for the medical images. Hippocampus is an essential part of the
246 brain. Human typical activity is based on the Hippocampus features. It takes several hours for a doctor to
247 physically section the Hippocampus. In this research, a improve method is used to separate the hippocampus
248 region, based on the watershed segmentation methodology. Using two methods, the brain images were
249 translated to binary form. The first solution is principles of block say, mask and marking and the second
250 method is concept of top hat, mask and marking. But some portion of the image is found to contain holes
251 that disrupt the segmentation phase. The image hole filling strategies are applied to solve this issue, and
252 relevant components are grouped into linked modules. The type study of the function of the hippocampus
253 may aid in the analysis of Alzheimer's disease (AD).

254 **2.2 Existing Methodology and its Disadvantages**

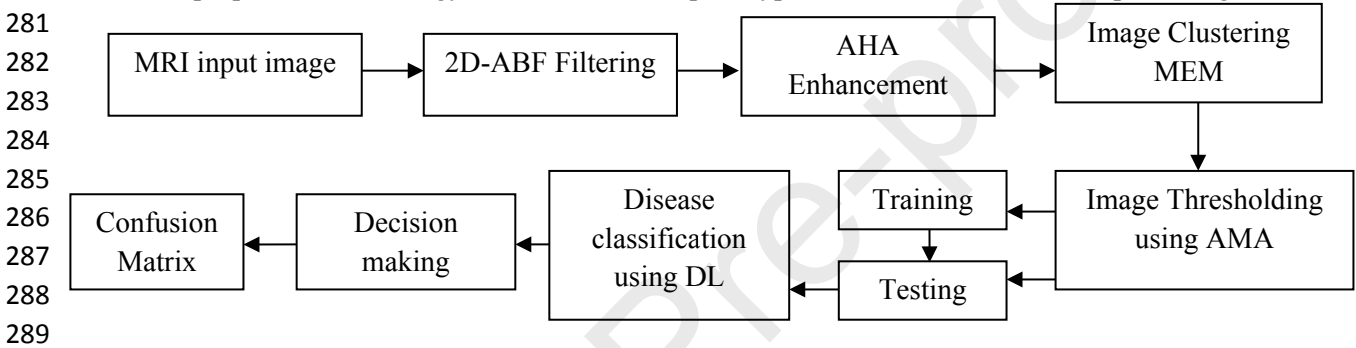
255 The existing method is to continuously separate regular tissues and irregular tissues through images of the
256 MRI tumors. Such MR brain images are observed to be distorted with Strength in objects of homogeneity
257 that induce excessive variance in strength and noise that impair the output of brain image processing. Due
258 of this type of substances one form of normal tissue in MRI is wrong classified as another standard tissue
259 which contributes to diagnostic error. The approach involves of preprocessing using 2D wrapping-based
260 Curvelet transformation for eliminating noise with adjusted contextual fuzzy C means procedure implies
261 taking into consideration the spatial details and fragments of natural structures as the surrounding pixels
262 are strongly associated and often spontaneously construct up the original participation matrix. The cancer
263 cells are often segmented by method. The conventional method is not capable of finding Alzheimer disease.

264

265 **3. MATERIAL AND METHODS**

266

267 The proposed system is made up of four steps, which include pre-processing, segmentation of region of
 268 interest, extraction of features and classification of disease. The training MRI Brain image is given as input
 269 to the network during the training period and is exposed to all of the above mentioned steps. A classification
 270 model is chosen, and the extracted features are used along with the class labels to train a classifier. Now
 271 the algorithm turns into a classification algorithm. A test brain MRI image is information into the structure
 272 during the testing stage, and the image moves through all of the above steps mentioned. The qualified
 273 classifier now recognizes the characteristics of the test object and can add a class mark to the test object as
 274 whether 'affected disease' or 'unaffected disease' using the information it has previously acquired during the
 275 training process. The research introduces a modern predictive approach for segmenting the entire brain into
 276 image sequence using magnetic resonance (MR) and measuring its density to diagnose disease. The relevant
 277 MRI brain images have been collected from the website of the Alzheimer's Neuro-imaging Initiative
 278 (ADNI). In participants entire MRI brain T1-weighted MRI was considered at 1.5 T level as given in the
 279 specification. The proposed automated clustering approach is considered on the image numerical anatomy
 280 and our proposed methodology is named as "head prototype" to restrict the MRI brain pixel range.



290 **Figure 1: Architecture diagram for proposed methodology**

291

292

293 3.1 MRI brain image Pre-processing

294

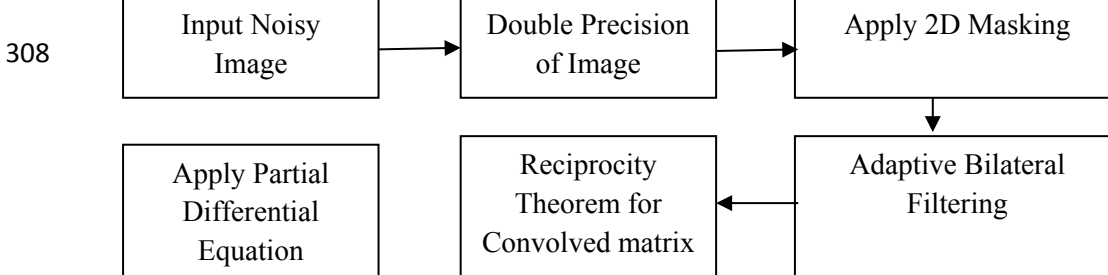
295 Figure 1 shows overall architecture of proposed methodology. The MRI image preprocessing technique is
 296 fulfilled with two techniques called image restoration and image enhancement. The image restoration of
 297 image is completed using 2D Adaptive Bilateral Filter (2D-ABF) algorithm. The 2D-ABF is used to
 298 eliminate unwanted noises like speckle noise, binary noise and random noise.

299

300 The 2D ABF is used to filter noises without degradation of original information content in MRI image. The
 301 image quality enhancement technique can be proposed using 2D Adaptive Histogram Adjustment (2D
 302 AHA) algorithm. The 2D AHA is used to enhance visual contrast and brightness for enhancing image
 303 consistency. The gray image is the useful format for MRI brain image segmentation. If it chooses MRI
 304 color image, it has to be converted from color image to gray image. The MEM algorithm will cluster
 305 abnormal pixels on gray images.

306

307



308

309

310



311



312

313

314

315 **Figure 2: Block diagram of 2D-ABF**

316 **3.2 Image Restoration using 2D Adaptive Bilateral Filter (2D-ABF)**

317

318 The figure 2 shows the proposed block diagram of image filtering using 2D-ABF. De-noising has often
 319 been a research priority and yet there is still scope for progress, particularly when it comes to image de-
 320 noising. When high frequency distortion is to be extracted from the distorted image, the basic temporal
 321 filtering of a distorted image can be effective. The biggest problem connected with this is the complexity
 322 of the calculation involved in making the convolution. The wavelength-based de-noising approaches use
 323 low-pass filtering to remove most high-frequency elements in attempt to de-noise the signal, as the noise is
 324 scattered over all wavelengths. It is generally not successful though, because it disrupts both noise and other
 325 elevated-frequency image characteristics, leading in an excessively smooth denoted image. The goal of
 326 image de-noising is to eliminate the noise whilst preserving as much clarity as possible of the essential
 327 image features such as boundaries. In the existence of exponential noise, vector filters, which comprise of
 328 transforming the image with a steady vector to produce a linear mixture of neighborhood values, is
 329 commonly used for noise reduction.

330

331 It can therefore create a blurry and smooth image with inadequate approximation of features and insufficient
 332 noise suppression. Gaussian-based filters are especially important as their forms are easily defined and both
 333 the forward and reverse Fourier transformations of a Gaussian function are true Gaussian structures.
 334 Alternatively, because the frequency domain filter becomes smaller, the temporal domain filter would be
 335 broader and would modulate the low frequencies leading in improved smoothing / blurring. Such Gaussian
 336 filters are traditional linear filters which were commonly used to de-noise images. The suggested image de-
 337 noising system utilizes the 2D Adaptive Bilateral Filter. A disparity between the initial image and its de-
 338 noised version indicates the algorithm's erased noise, which is considered process noise. The vibration of
 339 the system will sound like a stimulus in theory. Although even good quality images have some noise, it
 340 makes sense to test some de-noise approach in this manner, without the conventional trick of "using noise
 341 and then deleting it". Precisely, it is known by

342

343

$$MN = A - IF \quad (1)$$

344

345 where, A is the initial (not inherently noisy) image, and IF is the de-noising driver output for an input image
 346 A. Applying the bilateral filter to the noisy image combines the distortion together with the image
 347 information while maintaining the borders / sharp borders very well given the normal distortion variance is

348 less than the opposite edges. His process interference in Gaussian filter is negligible in harmonic sections
 349 of the image and very high close borders or texture, where the Laplacian cannot be low. Consequently, in
 350 flat regions of the image the Gaussian convolution is ideal but the borders and shadow are distorted. To
 351 obtain what the bilateral filter takes out of the distorted image, the system noise concept is redefined as the
 352 gap between the distorted image and its opposed value. So, Eq. (1) is expressed as

$$353 \quad MN = I - IF \quad (2)$$

354 where, $I = A + Z$ is A distorted image acquired by destroying the initial image A by a white Gaussian
 355 distortion Z and IF is a Bilateral filter source for an input image I. As all noise and image information have
 356 been extracted by the bilateral filter by combining the pixels, the process noise should comprise of distortion
 357 and image information together with certain borders. The distortion of the system due to Gaussian filtering
 358 would have better borders relative to that of bilateral filtering because the borders are maintained by filtering
 359 spectrum (π). The process noise MN is a mixture of image information D and a white Gaussian distortion
 360 N.
 361 N.

$$362 \quad MN = D + N \quad (3)$$

363 Now the challenge is to approximate the information image D, which has just the actual image attributes
 364 and edges/sharp borders that Bilateral filter eliminates, as reliably as necessary according to certain
 365 parameters and is merged with the Bilateral filtered image IF to get a stronger de-noise image with info. In
 366 class Wavelet, Eq. (3) can be replicated as

$$367 \quad Y = W + N_w \quad (4)$$

368 Where Y is a distorted wavelet coefficient (method noise), W is the real wavelet coefficient (detailed image)
 369 and N_w is Gaussian distortion free.

370 The noisy images $I \in R^{M \times N}$ were first filtered using 2D-ABF. In this filtering technique, the image
 371 $I(m, n)$ is convolved using function $u(m, n)$ using the following equation

$$372 \quad u(m, n) = \iint_{\Omega} I(\xi, \eta) g(m - \xi, n - \eta) d\xi d\eta \quad (1)$$

373 In our work, we have employed ABF function family. It is defined as follows

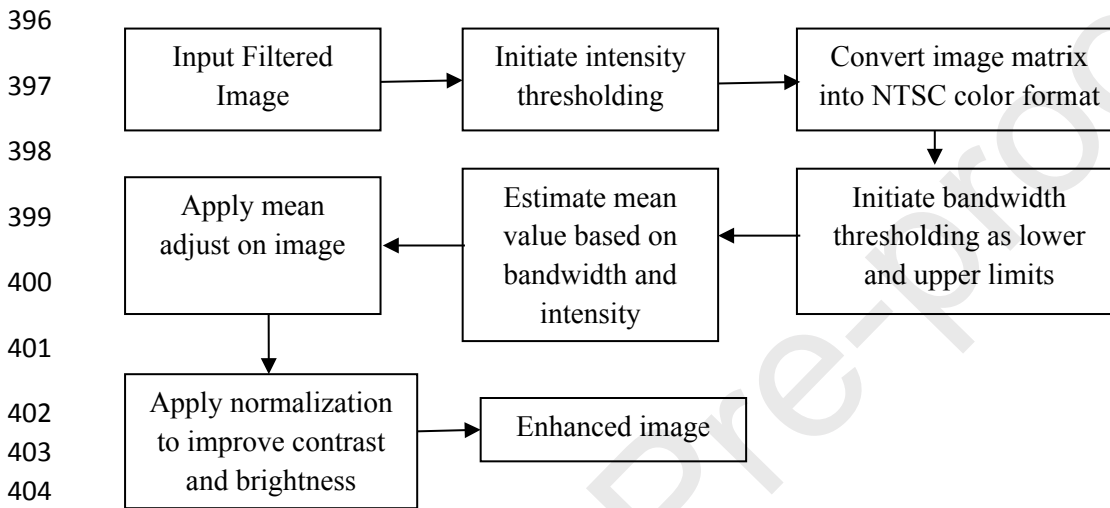
$$374 \quad g_{\lambda, \theta, \phi}(m, n) = e^{-((m^2 + \gamma^2 n^2)/2\sigma^2)} \cos(2\Pi \frac{m'}{\lambda} + \phi) \quad (2)$$

375 Here, $m' = m \cos \theta + n \sin \theta$, $n' = -m \sin \theta + n \cos \theta$, $\sigma = 0.56\lambda$ and $\gamma = 0.5$. Here, σ represents the
 376 scaling factor and θ represents the orientations of the filter functions. Thus, filtered images $I^F \in R^{M \times N}$
 377 were obtained by convolving input images with the function defined in Equation (2).

384 3.3 Image Enhancement using 2D Adaptive Histogram Adjustment (2D-AHA)

385

386 Figure 3 shows block diagram of 2D- Adaptive Histogram Adjustment. 2D Adaptive Histogram Adjustment
 387 (2D-AHA) is a machine-based type of image analysis used to boost or increase image intensity. AHA is
 388 ideally used for natural and therapeutic images. In this approach, it is done independently on sub-images,
 389 rather than implementing map or conversion to the entire image. AHA implements a method to correctly
 390 run the sub-image and merge it. Image quality improvement technique introduced in image histogram
 391 adjustment methodology to boost the over-amplification of noise issue occurring. This is distinct from
 392 normal histogram correction since it operates on specific segment of the MRI image quality being improved
 393 by multiple histograms all relative with a single region of the image then utilizing to reallocate image quality
 394 metrics like brightness or contrast calculation. AHA rather than normal histogram equalization increases
 395 the contrast of an image in which it provides rather clarity but also appears to intensity the distortion.



406 **Figure 3: Block diagram of 2D-AHA**

407 3.4 Proposed System

408 Step 1. Input (MRI image) is interpreted or perused.

409 Step 2. Change the MRI image into MRI at Gray point.

410 Step 3. To maximize the image quality, add or conduct the Histogram Equalization technique to the
 411 reference image.

412 Step 4. Take the improved-image histogram.

413 Step 5. Consider or execute the Local Equalization Histogram (LHE). Apply method for improving image
 414 contrast on the input image (MRI image).

415 Step 6. Step 4 has to be repeated.

416 Step 7. Enable or execute Adaptive Histogram (AHA) Adjustment. Apply method for improving viewpoint
 417 intensity on the reference image (MRI viewpoint).

426

427 Step 8. Do again step 4.

428

429 Step 9. To improve image quality, apply or execute the quality dependent adaptive histogram equalization
430 technique on the input image.

431

432 Step 10. Repeat step 4

433

434 **Pseudo code**

435

436 **Start**

437 Read MRI image

438 Apply Filtering with 2D- ABF

439 Apply Enhancement using AHA

440 Clustering for pixels

441 Segment region of interest

442 Estimate features

443 DL classification

444 **END**

445

446 **3.5 Alzheimer segmentation using Modified Expectation Maximization (MEM)**

447

448 Firstly, the principle of Expectation-Maximization is used to approximate the MRI information spread.
449 Category number is determined by the Bayesian Criteria of information. The Highest Probability is used to
450 group the pixels in images into the closest section. The consistency of the approach introduced is separate
451 of the original calculation and can be used in unsupervised clustering of the data. The Gaussian Mixture
452 Attributes of the MRI was initialized using the K-means method. Expectation maximization method is
453 implemented, and the Bayesian criterion is used to calculate the mixed model type numbers. This approach
454 sets the calculation of parameters and the collection of templates in one step and that is a clustering that is
455 completely unsupervised. Gaussian Mixture system is briefly implemented in the second section, and
456 approach is suggested based on the methodology 'Expected Total Bayesian Information Criterion.' A full
457 system of clustering shall be provided in the third section. The fourth element is the analysis, actual MRIs
458 are used in the clustering process and the findings indicate utility of the procedure in this research. The K-
459 means algorithm performed initial clustering. The phase in measurement may be described as:

460

461 Step 1. Start Select the original segmentation centers by the number of groups k.

462

463 Step 2. Categorized the pixel details are given into the category whose middle has the least pixel size.

464

465 Step 3. Start. Calculate the mean of the pixel values inside the class after a classification process.

466

467 Step 4. Unless the terms with the clusters have the same meaning, the present designation is the product of
468 clustering of the K-means.

469

470 Step 5. Edit the meaning of the clusters by means of the current level, and perform step 2.

471

472 Modified Expectation Maximization algorithm relies heavily on activation of clustering of pixels in various
 473 regions in image based on gradient. Using the calculation of Peak Probability to determine the final choice
 474 is a standard method, but it introduces heavy workload to the calculation. In this research, the mixture
 475 specifications are initialized using average K process. The explanation for utilizing Gaussian mixture is the
 476 complexity of calculating class level. Too many approaches presume that the amount is explicitly identified,
 477 that is, the amount of the type of images is decided by clustering. Clearly it is a process which is regulated
 478 or semi-supervised. A selection criterion for the model Bayesian Information Criteria (BIC) is used in this
 479 work to solve this issue. Clustering Methodology comprises of two steps: class approximation is the first
 480 step. The 'Expected Limit with Bayesian Criterion' approach is applied to approximate the numbers of the
 481 mixing variables and Gaussian elements. The second stage is sorting by pixels. According to the Maximum
 482 Likelihood rule per pixel is categorized towards a certain class.

483

484 **Expectation step:**

485 The probability that a pixel at $I^E(u, v)$ belongs to a particular Gaussian G_i with mean μ_i and standard
 486 deviation σ_i is given by

$$487 \quad P_{uv}^i = \frac{\exp\left(-\frac{(I^E(u, v) - \mu_i)^2}{2\sigma_i^2}\right)}{\sum_{j=1}^V \exp\left(-\frac{(I^E(u, v) - \mu_j)^2}{2\sigma_j^2}\right)} \quad (6)$$

488

489 **Maximization step:**

490 In this step, the values of mean μ_i and standard deviation σ_i of the Gaussian G_i are estimated again using

$$491 \quad \mu_i = \frac{1}{Z} \sum_{u,v} P_{uv}^i I^E(u, v) \quad (7)$$

$$492 \quad \sigma_i = \sqrt{\frac{\sum_{u,v} P_{uv}^i (I^E(u, v) - \mu_i)^2}{Z}} \quad (8)$$

493 The above two expectation and maximization steps are iterated until convergence state is achieved.
 494 The quality of clustering result obtained mainly depends on the initial values of the EM algorithm. In a
 495 conventional EM algorithm, these initial values are obtained using k-means algorithm. To further improve
 496 the accuracy and reliability of clustering result, in this work, we propose novel Enhanced Expectation
 497 Maximization algorithm. In this algorithm, instead of using k-means, the initial values are computed using
 498 Fuzzy C Means Clustering [36]. That is, the initial values are computed using

$$499 \quad J = \sum_{i=0}^{255} \sum_{q=1}^C f_{iq} d(i, \theta_q) \quad (9)$$

500 where f_{iq} refers to the fuzzy membership between pixel x_i and histogram of cluster with center θ_q and
 501 $d(i, \theta_q)$ refers to the distance between pixel x_i and histogram of cluster with center θ_q . The output of
 502 clustering step is represented as $I^C \in R^{U \times V}$.

503 3.6 Threshold using Adaptive Mean Shift (AMS)

504

505 Threshold methodology plays an important role in segmenting images and identifying trends. It's a method
 506 of splitting an image into various regions. The most stepped-forward method is to select appropriate some
 507 gray scale value as thresholds and categorize the image into more than one area. Two major classes are
 508 categorized into automated threshold techniques: global and local. A constant pixel values for the whole
 509 image is used in global approaches, while thresholds shift dynamically in local techniques. Though both of
 510 these strategies refine a criteria feature based on knowledge derived either from the development of
 511 histograms or from spatial distribution. One of the well-known and generally recognized adaptive threshold
 512 techniques, AMS threshold process, is focused on differentiate analysis to determine the highest class
 513 separable and is used to do histogram-based image threshold efficiently. AMS threshold ensures effective
 514 clustering by taking into consideration all pixels with a category value. Within the standard Fuzzy C Means
 515 the output threshold is contingent on the input threshold that has been randomly set, thus a suitable initial
 516 threshold is found within order to solve the complexities. The variable chosen for Fuzziness is the gray
 517 color values. Abnormal pixels separation is determined by conducting the threshold algorithm Fuzzy c
 518 means preceded by the hardening system. Fuzzy threshold is an enhancement for edge detection of the
 519 fuzzy clustering by including only the relevant features as a function. For fuzzy c-means which reduce
 520 objective functions.

521

522 **Input:**

523 Clustered image $I^C \in R^{U \times V}$.

524 **Output:**

525 Segmented image $I^S \in R^{U \times V}$.

526 **Steps:**

527 1 Divide the entire image $I^C \in R^{U \times V}$ into non-overlapping blocks of size $n \times n$.

528 2 Compute the histogram of each block B_i .

529 3 Identify the highest two peaks P_1 and P_2 in the histogram of each block.

530 4 The threshold T_i for block B_i is computed as

$$531 \quad T_i = \frac{P_1 + P_2}{2}$$

532 5 Segment the pixels $I_i^C(u, v)$ in block B_i using

533

$$I_i^S(u, v) = \begin{cases} 1; I_i^C(u, v) \geq T_i \\ 0; I_i^C(u, v) < T_i \end{cases}$$

534 **3.7 Feature Extraction using 2D-GLCM**

535

536 At this process, the feature report based on a biased image is quickly classified as normal and abnormal for
 537 extraction of features. Feature extraction is a method to depict the raw image to a segment that requires
 538 removal from the MRI image by classifying the characteristics. Feature extraction shows a reduction in the
 539 amount of data required to reliably defining broad database the characteristics used as inputs to identify and
 540 are positioned in the class described. The objective of extraction of the feature is to decrease the actual
 541 information by evaluating the beneficial property, or qualities that differentiate between one sample is
 542 placed and the other. Taking into account numerical feature vectors are valuable for indexing and detection
 543 of similar images. The texture function offers details on the characteristics of image strength at the diffusion
 544 stage such as homogeneity, softness, angularity, and contrasting. Statistical texture features consisting of
 545 mean, kurtosis, variance, image energy, standard deviation, skewness, entropy, and smoothness are
 546 computed based on the likelihood and allocation of the pixel level intensity.

547

548 Analysis of textures effectively distinguishes natural from irregular materials for human sensory perception
 549 from deep learning. It also creates differentiation among regular and malignant tissues, which might not be
 550 noticeable to human eyes. It improves precision by selecting effective early diagnostic comparative
 551 characteristics. During the initial step, data from the histogram of pixel intensity was obtained from the
 552 first-order statistical textural information associated and grey - level frequencies were evaluated at arbitrary
 553 image locations. It does not find association among pixels, or co-occurrences. In the next step, the textural
 554 evaluation-features of the second order were obtained based on the likelihood of pixel values at arbitrary
 555 ranges and over whole image configurations. Since, consistency of a classification method is dependent
 556 primarily on the correct selection of the function, a sufficient range of attributes needs to be defined. A
 557 feature matrix 2D-GLCM is applied in this classification procedure that is a mathematical approach that
 558 allows use of the pixel temporal association. By applying the GLCM, it is figure out which attributes are to
 559 be created depending on the cluster of a pixel. The research is done by guiding the distribution of 2D-
 560 GLCM features in such a way and suggested a series of statistics that are invariant to rotation. The scalar
 561 invariant attributes of rotation may be derived from vectors of co-occurrence by taking the average and
 562 distribution of each form of function over the four shapes that are used. Another type of definition of the
 563 texture is the gray-level variation data, which is directly linked to 2D-GLCM. A matrix of co-occurrence,
 564 also called a distribution of co-occurrence, is specified over an image to be the spectrum of co-occurring
 565 elements at a defined offset. It describes the structural association of distance and angle over an image sub-
 566 region of similar scale. The 2D-GLCM is formed from an image on a gray level. The 2D-GLCM is
 567 measured how much a gray-level pixel value appears horizontally, vertically, or diagonally to neighboring
 568 pixels with the value. The 2D-GLCM matrix could be a known statistical procedure for obtaining texture
 569 details from images in the second order. One of the most common and successful types of characteristics
 570 in texture evaluation is the 2D-GLCM vector. 2D-GLCM is the vector of all quantities for all gray level
 571 couples for a region identified by a user set frame. For this process, rather than the original gray-level pixel
 572 quantities, attributes are determined based on the absolute discrepancies between couples of gray-lines or
 573 mean 2D-GLCM lines. This feature makes the figures a little more reliable for differences of lighting than
 574 in the GLCM situation. The vector of the frequency of the gray level co-extracts from the above images.

575 For this research classification may be identified as the recognition function within which a collection of
 576 category the image belongs, either regular or impaired by Alzheimer disease. The recognition decision-
 577 making functions can be effectively achieved by utilizing Deep Learning (DL).

578
 579 It is computed as

$$580 \quad G(m, n) = \frac{\#\{(m_1, n_1), (m_2, n_2)\} \in S \mid f(m_1, n_1) = g_1 \ \& \ f(m_2, n_2) = g_2\}}{\#S} \quad (10)$$

581 Using this technique several statistical features like contrast, energy, homogeneity, correlation was
 582 extracted.

583 **Angular second moment:**

584 Angular second moment represents the uniformity of the distribution of the image. It is computed using the
 585 following formula

$$586 \quad A_{sm} = \sum_m^M \sum_n^N G(m, n)^2 \quad (11)$$

587 **Correlation:**

588 Correlation value indicates the similarity of the texture of the image in the two perpendicular directions
 589 namely, the horizontal and the vertical directions. It is computed using

$$590 \quad C_{or} = \frac{\sum_m^M \sum_n^N (m - \bar{x})(n - \bar{y})G(m, n)}{\sigma_x \sigma_y} \quad (12)$$

591 **Contrast:**

592 Contrast value indicates the variation of depth and smooth regions of the image and is computed as

$$593 \quad C_{on} = \sum_m^M \sum_n^N (m - n)^2 G(m, n) \quad (13)$$

594 **Entropy:**

595 Entropy is the measure of information content and is computed using

$$596 \quad E_{nt} = - \sum_m^M \sum_n^N G(m, n) I_g G(m, n) \quad (14)$$

597 **3.8 Alzheimer disease classification Deep Learning (DL)**

598
 599 The DCNN is derived from CNN technique. DCNN is nothing but the multiple stacked CNN model. The
 600 multiple stacks of layers will provide better recognition efficiency. Alzheimer's disease is divided into with

601 2 types: benign and malignant. For these cases, effective and accurate disease diagnosis and care plan
602 contributes to better quality of life and a longer life expectancy. Using DNN is one of the most functional
603 and effective approaches [20]. A DCNN was used to diagnose a disorder through images from body MRI
604 images. The suggested methodology is used by CNN to classify and characterize the disorder from brain
605 scans. The key distinction among the neural network's major channels with the conventional neural network
606 is that they are able to retrieve the attribute from each image dynamically and globally. These types of
607 networks take the form of neurons that can be learnt with weights and biases. For recovery functionality
608 the deep learning algorithm is used. The used algorithm was the clustering algorithm implemented to the
609 data set, and the images are then implemented to the DCNN. Results indicated that the approach proposed
610 was successful [21]. The objective of obtaining the property before implementing to the DCNN is to
611 evaluate fatty masses as disorder in some images, or the disorder is mistakenly regarded as fat in some
612 images and should have expanded medication errors. Extracting the parameter first and then adding the
613 DCNN results in better network performance and enhanced precision. Deep learning is one of the most
614 current practical ways of learning machines [22]. To put it another way, learning is called architecture deep-
615 seated. In fact, those implementations are the same old nerve systems that have become DNN. Such
616 networks are data based and function creation is performed automatically and does not mess with it, so
617 that's just what makes such networks reliable so outstanding efficiency in various fields. This is in essence
618 a deep learning of a series of nerve related strategies that learns features dynamically from our own input
619 results. The CNN is a specific kind of DNN whose framework is motivated by the perception cortex of cat
620 genetics. The CNN consists of many levels and has a hierarchical framework [23]. Input layer, output layer,
621 convolution layers, pooling layers, standardization layers and Totally Connected layers are all used in CNN.
622 CNN is distinctive in terms of the amount of layers used, the scale, amount of images and the form of kernel
623 function used. The parameters are selected in the CNNs, centered experimental results and experimentally
624 on trial and error [24]. In other terms, each CNN consists of many layers in which the key layers are the
625 Convolutional layer and the Sub-sampling layer added in the following points:

626
627 1) Convolution layer: Standard parameters have defined values such as metrics are essentially the same as
628 other sections of the image. It implies that learned characteristics from one segment of the image will be
629 added to other parts as well, and identical characteristics are included in all sections of the image. After the
630 system of the application, the Convolutional layer functions are used to classify images [25].

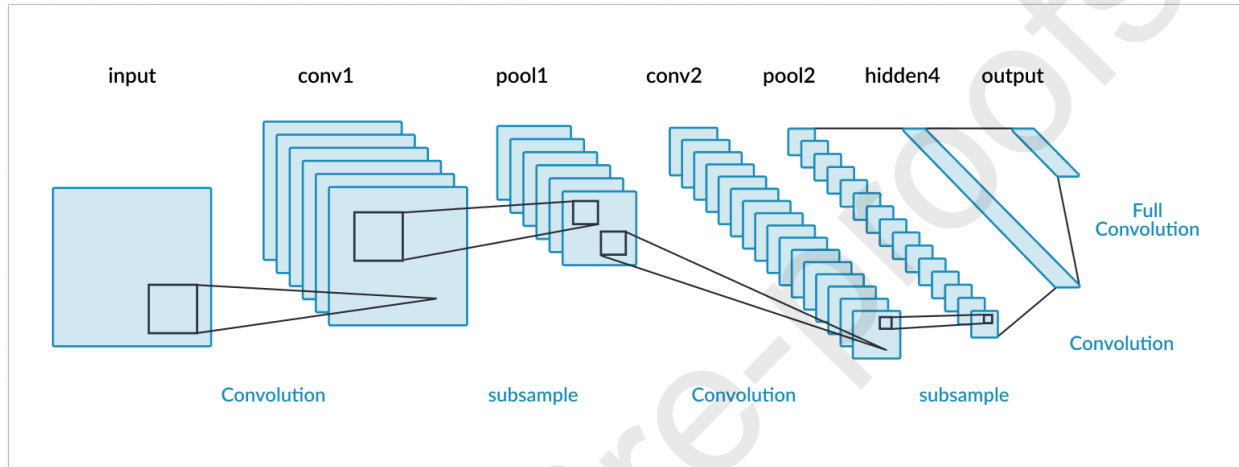
631
632 2) Sub-sampling layer: This layer functions are conducted to decrease the complexity of the image input.
633 It obtains a position matrix from the layer at the end of the DCNN. The process of aggregation or Sub-
634 Sampling is known as the mean pooling or peak pooling [26].

635
636 In a few instances, certain regions of fat in the images are incorrectly identified as sickness, or the physician
637 does not recognize the disease; the most precise diagnosis relies solely on the abilities of the physician. For
638 this paper the DCNN was used by brain scans to diagnose illness [27]. Extra margins of the images taken
639 from the imaging centers are included. Both margins have been clipped to keep the images from producing
640 noise. Some of the key factors for utilizing and integrating the extracting features strategy with the DCNN
641 are to recover the object extraction of the images to improve the network's reliability. In order to enhance
642 network accuracy, a new strategy which is a mixture of cluster analysis for decomposition of feature and
643 DCNN is presented in this research, as per the results of the DCNN on the initial images [28].

644

645 In DCNN, we have used transfer learning strategy that is used for training on issues similar to the same
 646 issue that may be resolved. Multiple stacks of layers through the training model can be used in a training
 647 model on the classification [29].

648
 649 The images were originally added to the CNN without any form of extraction of features. The DCNN
 650 architect was used to recognize and categorize images consisting of 5 Convolutionary layers and 3 layers
 651 of sub-sampling layers, standardization layers, standardization layers, Fully Connected layers, and
 652 ultimately classification layers [30]. The layers are fully connected, with 4096 neurons. In this layer, it has
 653 two classes: patient with brain disease, and regular patient. The DCNN used appears in figure 4.



654
 655 **Figure 4: Architecture of DCNN**

656
 657 Figure 4 shows architecture diagram of DCNN. In this research DCNN architecture is implemented
 658 to classify Alzheimer disease. Experimental findings reveal that our innovative DCNN design produces
 659 optimal efficiency and beats most of the cutting-edge systems performance. The result clearly shows the
 660 successful effectiveness and benefits of the proposed two-stage transfer learning strategy, as well as the
 661 possibilities of learning knowledge from MRI data.

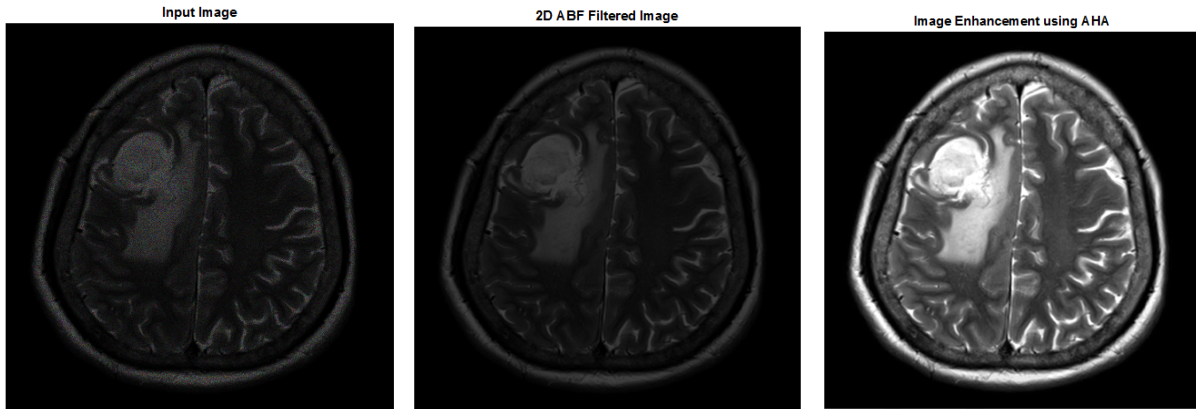
662 4. RESULTS AND DISCUSSION

663
 664
 665 This segment describes the real MRI image using proposed methodology experimental results are
 666 discussed. The experiments are done based on different standard of gray-scale MRI images with different
 667 size. The MRI images are corrupted by salt and pepper noise, speckle noise and random noise produced by
 668 MRI scanning devices as shown in figure 5 (a). The de-noising process is done based on these three noise
 669 aspects. The 2D Adaptive Bilateral Filter (2D ABF) is applied to noise corrupted image in order to remove
 670 all noises without degradation of original content of image as shown in figure 5 (b). To authorize the
 671 suggested methodology, their presentation are evaluated in terms of visual quality, PSNR and MSE are
 672 computed and tabulated using proposed algorithm called 2D ABF.

673
 674 In the figure 5 (a) MRI brain input image is shown for processing further to segment ROI. The 2D
 675 ABF filter is applied to eliminate noises such as Gaussian noise, binary noise and random noise are
 676 eliminated as shown in figure 5 (b). The filter image is further processed to improve quality of image using
 677 AMA algorithm. The contrast and brightness is improved using AMA algorithm as shown in figure 5 (c).

678 The PSNR and MSE are calculated for existing preprocessing techniques and proposed preprocessing
 679 technique. The values are tabulated in Table 1.

680



681

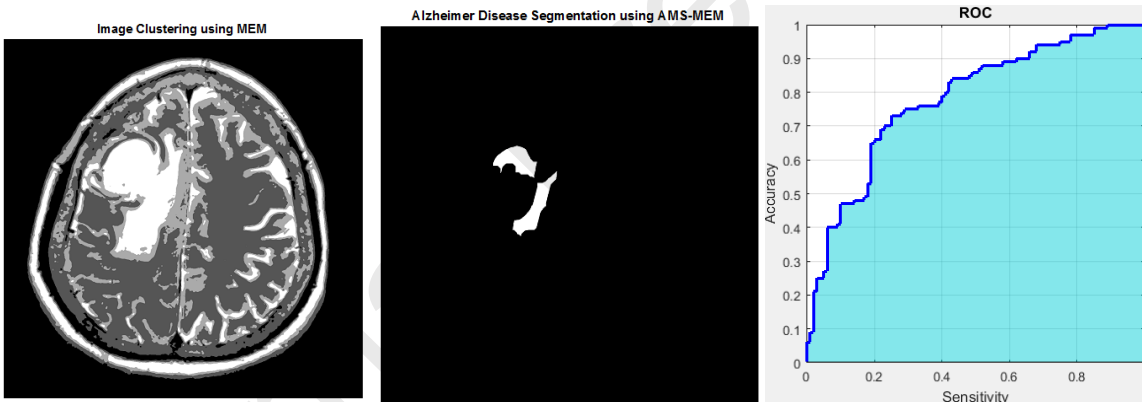
682

683 **Figure 5: (a) Input MRI image, (b) 2D ABF Filtered Image, (c) Image Enhancement using AHA**

684

685 The figure 5 (c) shows enhancement image using Adaptive Histogram Adjustment (AHA) by improvement
 686 of contrast and brightness. The quality of image is improved using AHA algorithm.

687



688

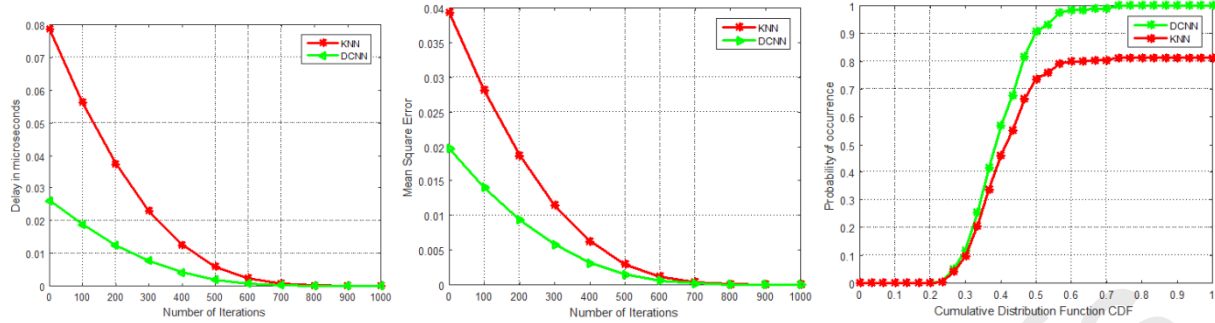
689

690 **Figure 6: (a) Image Clustering using AMS MEM algorithm, (b) Alzheimer disease segmentation**
 691 **using AMS MEM algorithm, (c) ROC Curve**

692

693 Figure 6 (a) shows clustered image using AMS-MEM algorithm. The different intensity pixels are grouped
 694 using AMS-MEM algorithm. The Bayesian Threshold technique is applied to AMS-MEM algorithm in
 695 order to segment Alzheimer disease as displayed in figure 6 (b). The figure 6 (c) shows ROC curve of
 696 DCNN classifier. The 6 (c) shows Area Under Curve (AUC) value is 98 %.

697



698
699 **Figure 7: (a) Delay minimization of DCNN, (b) MSE of KNN and DCNN, (c) Probability of**
700 **Occurrence**

701
702 Figure 7 (a) displays delay (Latency) estimation for KNN and DCNN classifier approaches. The DCNN
703 classification delay is considerably decreased thus compared to KNN. Figure 7 (b) shows Mean Square
704 Error (MSE) estimation for KNN and DCNN. The MSE of DCNN is lesser than KNN. Probability of
705 occurrence is represented for KNN and DCNN classifier in figure 5 (c). The table 1 shows the numerical
706 values comparison between existing filters and proposed 2D ABF. The table 2 shows various features
707 estimated using GLCM algorithm. AD disease image and normal image are compared and listed in the
708 table 2.

709

710 **Table 1 Image Quality Measurement**

711

S. No	Algorithm	PSNR	MSE
1	2D Median Filter	32.9383	2.8383
2	2D Bilateral Filter	38.3989	1.3989
3	2D Adaptive Bilateral Filter	47.3989	0.0938

712

713 **Table 2 GLCM Feature extraction**

714

S. No	GLCM Features	Alzheimer Disease (AD) Image	Normal Image
1	Entropy	0.4544	1
2	Auto correlation	0.8333	1
3	Contrast	3.8498	9.9309
4	Cross Correlation	1	0
5	Cluster Prominence	5.9383	9.0393
6	Cluster shade	5.0909	9.6353
7	Energy	2.9389	8.3988
8	Homogeneity	1.9389	9.3987
9	Dissimilarity	9.3876	0.9387
10	Energy	1.9333	9.3987
11	Maximum Probability	0	1

715

716 Table 1 shows image quality measurements using PSNR and MSE for various filters such as 2D Median
 717 Filter, 2D Bilateral Filter and 2D Adaptive Bilateral Filter. Compare to all three images, 2D ABF
 718 performance is better than all other filters. The AHA is applied to improve image quality. The proper
 719 preprocessing method is used to segment the ROI. The Table 2 shows various GLCM features are calculated
 720 for classification using DCNN. The table 3 shows precision and recall computation using True Positive
 721 (TP), True Negative (TN), False Positive (FP), and False Negative (FN) values.

722
723
724

725 **Table 3 Precision and Recall**

726 Testing 727 formula	Description	CM
728 1. Precision (P)	Classifier correctness.	$P = TP / (TP + FP)$
729 2. Accuracy (A)	Prediction algorithm accuracy.	$A = (TP + TN) / N$
730 Where N- Total No. of samples		

731
732

733
734 The confusion matrix is given below which forecast experimental results on a deep learning classification
 735 problem. The amount of right and incorrect forecasts are estimated with calculation ranges and given by
 736 every class. Table 4 shows the confusion matrix values of TP, TN, FP and FN.

737
738
739
740

741 **Table 4 Confusion Matrix**

742

	Class 1 Prediction	Class 2 Prediction
Class 1 Actual	TP	FN
Class 2 Actual	FP	TN

743
744

	Class 1 Prediction	Class 2 Prediction
Class 1 Actual	50	10
Class 2 Actual	5	100

745
746

Table 5. Performance evaluation using Jaccard Coefficient

Images	Coefficient of Jaccard		
	Fuzzy C Means (FCM) clustering	Fast Fuzzy C Means Clustering	Proposed MEM Clustering
1	0.3336	0.5783	0.9389

2	0.4837	0.5837	0.9382
3	0.4193	0.6938	0.8397
4	0.4684	0.6376	0.8376

747

748 Table 5 shows the performance evaluation using Dice Coefficient. From Table 5, the average value
 749 of Dice Coefficient for FCM clustering was 0. 4837. Similarly, the average value of Dice Coefficient for
 750 Fast FCM Clustering was 0. 6938. But the proposed MEM Clustering achieved a maximum Dice
 751 Coefficient of 0.9389. Thus, our proposed framework achieves best performance in terms of Dice
 752 Coefficient.

753 Table 6 Precision and Accuracy

754

755 Using table 6, precision and accuracy are estimated and tabulated as given below. In the table 5, the
 756 proposed classification is compared with K-nearest neighbor (KNN) algorithm. The KNN is the kind of
 757 supervised Machine Learning (ML) method that can be applied for both classification and regressive
 758 prediction issues.

759

760 Classification	Algorithms	Precision in %	Accuracy in %
761 ANN	KNN	82	84
762 DL	DCNN	97	96

763

764 The experimental results are given on different types of images such as normal and abnormal with various
 765 noise levels. The 2D Adaptive Bilateral Filter is used for de-noising and adaptive mean adjustment (AMA)
 766 is applied for image enhancement. The PSNR is calculated by applying the formula is,

$$767 \text{ PeakSignaltoNoiseRatio} = 10 * \log_{10} \left(\frac{255^2}{mse} \right) \text{ in dB}$$

768

769 Where, the MSE is estimated by using the below formula is,

$$770 mse = \frac{1}{I \times J} \sum_{i=1}^I \sum_{j=1}^J [\chi(i, j) - \hat{\chi}(i, j)]^2 \quad (15)$$

771

772 Pseudo code for ANN-KNN

773

774 The proposed DCNN classification technique is compared with ANN-KNN classification technique. ANN-
 775 KNN diverge the difference between a selection of new data and all learning data sets, and the minimum
 776 distance is found as better neighbor. The k value is calculated objectively, using Sorting error for the
 777 Learning sample. The ANN-KNN is one of the important classification techniques to given better accuracy
 778 and efficiency.

779

780 1. Initialize the training data and testing data

- 781 2. Select the range of K value
 782 3. For every position in testing data:
 783 - Estimate the Euclidean distance to each training data position
 784 - accumulate the Euclidean distances in a record and arrange it
 785 - decide the initial k position
 786 - allocate a class to the testing position using the significance of classes available in the selected
 787 positions
 788 4. End

789 **Pseudo code for DCNN**

790
 791
 792 for classification patterns
 793 % Feed Forward computation
 794 for each neurons (nn)
 795 for each weights vector of the neuron (nx)
 796 Estimate net using Sigmoid function
 797 end;
 798 Estimate deep convolution
 799 Estimate neuron output;
 800 Estimate neuron slope;
 801 end;
 802 for all outputs (no)
 803 estimate error;
 804 Deep convolution computation
 805 initial delta as slope;
 806 for all neurons preliminaryas of output neurons (nn)
 807 for the weights connected to other neurons (ny)
 808 multiply delta through weights
 809 sum the backpropagated delta at proper nodes
 810 end;
 811 multiply delta by slope (for hidden neurons);
 812 end;
 813 end;
 814 end;

815
 816 **Overall accuracy:**

817 Overall accuracy indicates the overall classification performance of the classifier.

$$818 \text{ Overall accuracy} = \frac{TP + TN}{TP + TN + FP + FN} \quad (21)$$

819
 820 where TP refers to true positives, TN refers to true negatives, FP refers to false positives and FN refers
 821 to false negatives.

822

823 Recall:

824 The recall ratio of number of positive cases is correctly classified to the total number of positive cases.

$$825 \text{ Recall} = \frac{TP}{TP + FN} \quad (22)$$

826 Precision:

827 The precision is the ratio of number of positive cases that are correctly classified to the total number
828 of cases classified as positive.

$$829 \text{ Precision} = \frac{TP}{TP + FP} \quad (23)$$

830

831 Specificity:

832 The specificity is the ratio of number of negative cases that are correctly classified to the total number
833 of negative cases.

$$834 \text{ Specificity} = \frac{TN}{TN + FP} \quad (24)$$

835

836 F-score:

837 The F-score is computes as

$$838 \text{ F-score} = 2 \times \frac{\text{Precision} \times \text{Recall}}{\text{Precision} + \text{Recall}} \quad (25)$$

839

840 The classification is also performed using traditional machine learning algorithms like KNN
841 and DCNN for comparison. Table 6 shows the results obtained in terms of overall accuracy. From
842 Table 5, we see that Logistic Regression algorithm produces the best results compared to all other
843 traditional classification algorithms.

844

845

846 5. CONCLUSION

847

848 The Computer Aided Diagnosis (CAD) system is proposed using various algorithms to detect and classify
849 Alzheimer disease on MRI real images. The Alzheimer disease a most threatening image and tool for testing
850 of disease is very costly. The automatic segmentation and classification of Alzheimer disease (AD) in MRI
851 brain images is implemented. The proper preprocessing is applied on the tool using 2D Adaptive Bilateral
852 Filter (2D ABF) and Adaptive Histogram Adjustment (AHA). The segmentation ROI is done using
853 Modified Expectation Maximization (MEM). The various image features are retrieved using GLCM and
854 the DCNN classification technique is used to classify normal and abnormal image. The accuracy of
855 classification is more than 98% using Deep Convolutional Neural Network.

856

857 FUTURE WORK

858

859 In future, CAD system may be applied for cancer cells identification by proper segmentation of Gray Matter
860 (GM), White Matter (WM) and CSF. The adaptive clustering technique can be applied to segment disease
861 region without pixels error. The DCNN can be applied to distinguish regular and anomalous MRI brain
862 images.

863

864 **ACKNOWLEDGEMENT**

865 The authors would like to thank [https://www.kaggle.com/navoneel/brain-mri-images-for-brain-tumor-](https://www.kaggle.com/navoneel/brain-mri-images-for-brain-tumor-detection)
 866 [detection](https://www.kaggle.com/navoneel/brain-mri-images-for-brain-tumor-detection) for providing dataset for doing research.

867 **REFERENCES**

868

869 [1].Wei Li, Yifei Zhao, Xi Chen, Yang Xiao, Yuanyuan Qin, “Detecting Alzheimer’s Disease on Small
 870 Dataset: A Knowledge Transfer Perspective”, IEEE 2018.

871 [2].Samsuddin Ahmed, Kyu Yeong Choi, Jang Jae Lee, Byeong C. Kim, Goo-Rak Kwon , Kun Ho Lee and
 872 Ho Yub Jung, “Ensembles of Patch-Based Classifiers for Diagnosis of Alzheimer Diseases”,
 873 doi:10.1109/ACCESS.2019.2920011.

874 [3]. Jun Zhang, Yue Gao, Yaozong Gao, Brent C. Munsell, Dinggang Shen, “Detecting Anatomical
 875 Landmarks for Fast Alzheimer’s Disease Diagnosis”, DOI 10.1109/TMI.2016.2582386, IEEE 2016.

876 [4]. M. A. Balafar, “New spatial based MRI image de-noising algorithm”, DOI 10.1007/s10462-011-9268-
 877 0.

878 [5]. Fabrizio Russo, “Validation of Denoising Algorithms for Medical Imaging”, Springer 2010.

879 [6]. Saritha Saladi , N. Amutha Prabha, “Analysis of denoising filters on MRI brain images”, DOI:
 880 10.1002/ima.22225, <https://www.researchgate.net/publication/319163534>.

881 [7]. Chiao-Min Chen, Chih-Cheng Chen, Ming-Chi Wu, Gwoboa Horng, Hsien-Chu Wu, Shih-Hua Hsueh,
 882 His-Yun Ho, “Automatic Contrast Enhancement of Brain MR Images Using Hierarchical Correlation
 883 Histogram Analysis”, DOI 10.1007/s40846-015-0096-6.

884 [8]. Raouia Ayachi and Nahla Ben Amor, “Brain Tumor Segmentation Using Support Vector Machines”,
 885 Springer 2009.

886 [9]. Samir S. Yadav and Shivajirao M. Jadhav, “Deep convolutional neural network based medical image
 887 classification for disease diagnosis”, Springer 2019.

888 [10]. P. Muthu Krishnammal and S.Selvakumar Raja, “Convolutional Neural Network based Image
 889 Classification and Detection of Abnormalities in MRI Brain Images”, IEEE 2019.

890 [11]. Krystyna Malik and Bogdan Smolka, “Modified Bilateral Filter for the Restoration of Noisy Color
 891 Images”, Springer 2012.

892 [12]. Jun Wang and Xiaohong Meng, “Employing the bilateral filter to improve the derivative-based
 893 transforms for gravity and magnetic data sets”, DOI: 10.1007/s11200-018-0162-y 4,

894 [13]. V. Anoop1 and P. R. Bipin, “Medical Image Enhancement by a Bilateral Filter Using Optimization
 895 Technique”, Springer 2019.

896 [14]. Rinkal Patel, Jun Liu, Kewei Chen, Eric Reiman, Gene Alexander and Jieping Ye, “Sparse Inverse
 897 Covariance Analysis of Human Brain for Alzheimer's Disease Study”, IEEE 2019.

898 [15]. Mostafa Amin-Naji, Hami Mahdavinataj and Ali Aghagolzadeh, “Alzheimer's disease diagnosis from
 899 structural MRI using Siamese convolutional neural network”, IEEE 2019.

900 [16]. Shanthi K J, Ravish D K and Dr. M Sasikumar, “Image segmentation an early detection to Alzheimer's
 901 disease”, DOI: 10.1109/INDCON.2013.6726006.


902 [17]. R. Thillaikkarasi1 and S. Saravanan, “An Enhancement of Deep Learning Algorithm for Brain Tumor
 903 Segmentation Using Kernel Based CNN with M-SVM”, Springer 2019.


- 904 [18]. G. K. Reynolds ; T. M. Nir ; N. Jahanshad ; G. Prasad ; P. M. Thompson , “Using the raw diffusion
905 MRI signal and the von Mises-Fisher distribution for classification of Alzheimer's disease”, 2014 IEEE
906 11th International Symposium on Biomedical Imaging (ISBI), DOI: 10.1109/ISBI.2014.6868048
- 907 [19]. Jun Zhang, Member, IEEE, Mingxia Liu, Member, IEEE, Le An, Yaozong Gao, Dinggang Shen_,
908 Senior Member, IEEE, “Alzheimer’s Disease Diagnosis using Landmark-based Features from Longitudinal
909 Structural MR Images”, 2168-2194 (c) 2016 IEEE.
- 910 [20]. Ramy A. Zeineldin¹ · Mohamed E. Karar² · Jan Coburger³ · Christian R. Wirtz³ · Oliver Burgert¹,
911 “DeepSeg: deep neural network framework for automatic brain tumor segmentation using magnetic
912 resonance FLAIR images”, Springer 2020, International Journal of Computer Assisted Radiology and
913 Surgery.
- 914 [21]. MRI brain dataset, <https://www.kaggle.com/navoneel/brain-mri-images-for-brain-tumor-detection>.
- 915 [22]. Estimation of Diaphragm Wall Deflections for Deep Braced Excavation in Anisotropic Clays Using
916 Ensemble Learning. Geoscience Frontiers. DOI: 10.1016/j.gsf.2020.03.003
- 917 [23]. Wengang Zhang, Chongzhi Wu, Haiyi Zhong, Yongqin Li, Lin Wang, “Prediction of undrained shear
918 strength using extreme gradient boosting and random forest based on Bayesian optimization” Geoscience
919 Frontiers, 2020.
- 920 [24]. Afshar, P.; Plataniotis, K.N.; Mohammadi, A. Capsule Networks for Brain Tumor Classification
921 Based on MRI Images and Coarse Tumor Boundaries. In Proceedings of the ICASSP 2019–2019 IEEE
922 International Conference on Acoustics, Speech and Signal Processing (ICASSP), Brighton, UK, 12–17 May
923 2019; pp. 1368–1372.
- 924
- 925 [25]. Byrne, J.; Dwivedi, R.; Minks, D. Tumours of the brain. In Nicholson T (ed) Recommendations Cross
926 Sectional Imaging Cancer Management, 2nd ed.; Royal College of Radiologists: London, UK, 2014; pp.
927 1–20. Available online: [https://www.rcr.ac.uk/publication/recommendations-cross-sectional-imaging-](https://www.rcr.ac.uk/publication/recommendations-cross-sectional-imaging-cancer-management-second-edition)
928 [cancer-managementsecond-edition](https://www.rcr.ac.uk/publication/recommendations-cross-sectional-imaging-cancer-management-second-edition) (accessed on 5 November 2019).
- 929
- 930 [26]. Mlynarski, P.; Delingette, H.; Criminisi, A.; Ayache, N. Deep learning with mixed supervision for
931 brain tumor segmentation. *J. Med Imaging* **2019**, *6*, 034002.
- 932
- 933 [27]. Amin, J.; Sharif, M.; Yasmin, M.; Fernandes, S.L. Big data analysis for brain tumor detection: Deep
934 convolutional neural networks. *Futur. Gener. Comput. Syst.* **2018**, *87*, 290–297.
- 935
- 936 [28]. Amin, J.; Sharif, M.; Raza, M.; Yasmin, M. Detection of Brain Tumor based on Features Fusion and
937 Machine Learning. *J. Ambient. Intell. Humaniz. Comput.* **2018**, 1–17.
- 938
- 939 [29]. Usman, K.; Rajpoot, K. Brain tumor classification from multi-modality MRI using wavelets and
940 machine learning. *Pattern Anal. Appl.* **2017**, *20*, 871–881.
- 941 [30]. Pereira, S.; Meier, R.; Alves, V.; Reyes, M.; Silva, C. Automatic Brain Tumor Grading from MRI
942 Data Using Convolutional Neural Networks and Quality Assessment. In *Understanding and Interpreting*


943 Machine Learning in Medical Image Computing Applications; Springer: Berlin/Heidelberg, Germany,
944 2018; pp. 106–114.


945
946 [31]. Farhi, L.; Zia, R.; Ali, Z.A. 5 Performance Analysis of Machine Learning Classifiers for Brain Tumor
947 MR Images. *Sir Syed Res. J. Eng. Technol.* **2018**, 1, 6.

948
949 **ABOUT AUTHORS**


950
951  **Dr. V. Sathiyamoorthi** (*Corresponding Author*) is currently working as an Associate
952 Professor in Computer Science and Engineering Department at Sona College of
953 Technology, Salem, Tamil Nadu, India. He was born on June 21, 1983, at Omalur in
954 Salem District, Tamil Nadu, India. He received his Bachelor of Engineering degree in
955 Information Technology from Periyar University, Salem with First Class. He obtained
956 his Master of Engineering degree in Computer Science and Engineering from Anna
957 University, Chennai with Distinction and secured 30th University Rank. He received
958 his Ph.D degree from Anna University, Chennai in Web Mining. His areas of specialization include
959 Machine Learning, Data Science, Web Usage Mining, Data Structures, Design and Analysis of
960 Algorithm and Operating System. He has published many papers in International Journals and
961 conferences. He has published many books and book chapters in various renowned international
962 publishers. He has also participated in various National level Workshops and Seminars conducted by
963 various reputed institutions.

964
965  **Dr. Ilavarasi A K** is currently working as an Assistant Professor in the School of
966 Computing Science and Engineering at Vellore Institute of Technology, Chennai, India.
967 She received her Bachelor of Engineering Degree from Amrita University, Master of
968 Engineering Degree with Distinction from Anna University and Ph.D. Degree from
969 Anna University. Her primary research interests include the areas of Privacy
970 Preserving Data Mining (PPDM) and Health Care Data Analytics. She has co-authored
971 a book on Fundamentals of Computing and has conducted various National level
972 workshops and Seminars. She is a Co-investigator of a grant received from Department of Science
973 and Technology, New Delhi, India.


974
975  **Prof. Murugeswari .K** received her B.E in Computer Science and Engineering and
976 M.Tech in Information Technology in 1996 and 2003, respectively, from Madurai
977 Kamaraj University and University of Punjab. She started her carrier as a lecturer in
978 1997 and continues her service in teaching field. She worked for 16 years as an
979 Assistant Professor in Thiagarajar College of Engineering, Madurai. Currently she is
980 working as an Associate Professor in Kalasalingam Academy of Research and
981 Education. Her research interests include information security, Steganalysis and Soft Computing
982 Techniques.

983
984  **Prof. Syed Thouheed Ahmed**, is with Dr. T Thimmaiah Institute of Technology, as
985 Assistant Professor in CSE, He was graduated in B.E Computer Science and Engineering

986 from Visveswaraya Technological University in 2013, M.Tech in Computer Science and Engineering
987 from REVA Institute of Technology and Management, now as REVA University, Bangalore in 2015.
988 Currently, He is Doctoral Fellow at School of Computers, Information and Mathematical Sciences, BSA
989 CRESCENT University, Chennai. Prof. Syed, has published 45+ research articles and papers in the field
990 of Machine Learning, Big Data Analytics, Telemedicine, Image and Video Processing, cloud computing
991 and IoT at reputed international and national journals and conferences. His work is sighted with
992 reputed publishers like Elsevier, Springer, Inderscience and IEEE. His research grant covers rupees
993 45 Lakhs from Central and State government of Karnataka and Tamil Nadu since 2015.

994  **Dr Arunadevi Baladhandapani**, an academican and a researcher, Dr.N.G.P Institute
995 of Technology, with research interests primarily in the domain of Pattern Recognition,
996 Embedded Systems, Robotics, and Remote Sensing with emphasis on Artificial
997 Intelligence, Biomedical Analytics and Learning -Recognition for Assistive Computer
998 Vision. She has co-authored a patent, various books chapters and research papers in
999 leading journals and conference proceedings. Has peer reviewed many international
1000 journals and an active member in various professional societies.

1001

1002  **Mr.K.Murali** received the B.Sc., degree in electronics from PB Siddhartha college of
1003 arts and science, AP, India, in 2003, the M.Sc. degree in electronics from PB
1004 Siddhartha Post graduate center, AP, India, in 2005, and the M.Tech., degree in
1005 electronics and communication engineering from VR Siddhartha engineering
1006 college, AP, India, in 2009.He is currently pursuing the Ph.D. degree in electronics
1007 and communication engineering, under the esteemed guidance of Dr.S.Siva Perumal
1008 at Vel Tech Rangarajan Dr.Sagunthala R&D Institute of Science and Technology, Tamilnadu, India.
1009 Since 2009 he has been an Assistant professor with the Vijaya Institute of technology for women, AP,
1010 India. He is the author of more than 49 research articles. His research interest includes the
1011 development of wireless communications 5G and beyond and optimization tools with Machine
1012 learning applications to next generation wireless standards.

1013

1014 **Cover Letter**

1015 **Dr V Sathiyamoorthi**

1016 **[04.06.2020]**

1017

1018 Dear Editor

1019 I/We wish to submit an original research article entitled "**A Deep Convolutional**
1020 **Neural Network (DCNN) based Computer Aided Diagnosis (CAD) System for the**
1021 **Prediction of Alzheimer's Disease in MRI Brain Images**" for consideration by
1022 **Measurement**. I/We confirm that this work is original and has not been published
1023 elsewhere, nor is it currently under consideration for publication elsewhere.

1024 We have no conflicts of interest to disclose.

1025 Please address all correspondence concerning this manuscript to me at
1026 sathyait2003@gmail.com

1027

1028 Thank you for your consideration of this manuscript.

1029

1030 Sincerely,

1031 Dr V Sathiyamoorthi

1032

1033

1034

CREDIT AUTHOR STATEMENT

1035

1036 **Sathiyamoorthi V:** Conceptualization, Methodology, Software, Visualization,

1037 **Sathiyamoorthi V** and **Ilavarasi A K:** Data curation, Writing- Original draft preparation.

1038 **Sathiyamoorthi V** and **Murugeswari K:** Formal Analysis, Investigation.

1039 **Sathiyamoorthi V** and **Syed Thouheed Ahmed:** Supervision.

1040 **Sathiyamoorthi V** and **Aruna Devi B:** Validation.

1041 **Sathiyamoorthi V** and **Murali K:** Reviewing and Editing

1042

1043 **Declaration of interests**

1044

1045 The authors declare that they have no known competing financial interests or personal relationships
1046 that could have appeared to influence the work reported in this paper.

1047

1048 The authors declare the following financial interests/personal relationships which may be considered
1049 as potential competing interests:

1050

1051

1052

1053

1054

1055